Journal of Hydraulic Structures
J. Hydraul. Struct., 2023; 6(3):66-87
DOI: 10.22055/jhs.2023.45051.1267

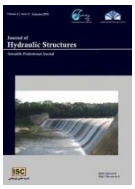

OPEN ACCESS

Transverse Velocities and Vortices in Compound Meandering Channel: Effect of Building Arrangement in the Floodplains

Mohammad Naghavi [1]
Mirali Mohammadi [2]
Ghorban Mahtabi [3]

Abstract

Numerical simulations were carried out in a compound meandering channel to investigate the effect of building arrangements in the floodplain on the flow field in the main channel. Three types of structural arrangements were used: structural obstacles parallel and perpendicular to the flow of the floodplain (MGT and MHT), and checkered structural barriers (MFT). The transverse velocities, flow angle and vortices along the half meander were measured. Numerical simulation results showed that the building arrangements in the floodplain can significantly change the transverse velocities and flow angle in the main channel. Near the convex arc of the apex sections (CS1 and CS7), the transverse flow velocity increased by changing the building arrangements from parallel to the floodplain flow (MGT1) to perpendicular to the floodplain flow (MHT1) (517% increase), but in the center of the main channel in the middle section (CS4), the transverse velocity decreases with the change of the arrangement from the parallel state (MGT1) to the perpendicular state to the floodplain flow (MHT1) (47% decrease). In the vicinity of the concave arc, in the apex sections (CS1 and CS7), the change of transverse velocity is insignificant due to the change in the arrangement. In the middle section (CS4), the maximum transverse velocity in cases MFT1, MGT1 and MHT1 decreases by 84%, 49% and 80% on average respectively, compared to the smooth floodplain (MAT). In the center of the middle section (CS4), the change of arrangement has the greatest effect on the flow angle, so that the lowest flow angle is observed for cases with the arrangement of buildings perpendicular to the floodplain flow and checkered (MHT and MFT). Also, in the middle section, the strength of vortices rotation increases significantly in the case of MGT1 compared to the case of MHT1.

Keywords: Compound meandering channel, Building arrangements, Transverse velocity, Vorticity, Flow angle.

Received: 20 October 2023; Accepted: 15 December 2023

[1] Department of Civil Eng., Faculty of Eng., Urmia University, P O Box 165, Urmia 57561-15311, Iran. (**Corresponding author**)
[2] Department of Civil Eng., Faculty of Eng., Urmia University, P O Box 165, Urmia 57561-15311, Iran.
[3] Department of Water Eng., University of Zanjan, Zanjan 45371-38791, Iran.

1. Introduction

Most natural rivers turn into compound meandering channels during floods, which have a main channel and one or two adjacent floodplains [1]. The flow mechanism in compound meandering channel is a complex three-dimensional flow in comparison with the straight channel [2]. During flood, the extreme exchange of momentum develops between the floodplains and the main channel. Furthermore, the flow direction in floodplain and main channel are not parallel so that the flow direction of the main channel is parallel to the sidewall of the meandering main channel [3]. In the compound meandering channel, the difference in flow velocity between the main channel and the floodplain leads to the creation of a shear layer between the two areas [4]. Also, due to the transfer of water between the main channel and the floodplain, an additional flow resistance is created [5]. In the compound meandering channel, the vortices created due to the momentum exchange are eventually moved downstream and the erosion and sedimentation pattern alter significantly [6-8]. In the last decades, many experimental and numerical studies have been conducted to investigate the flow characteristics and vorticity flow in compound meandering channels [2, 3, 8, 9]. The findings present that in compound meandering channels, the relative depth, roughness, cross sectional shape and sinuosity are the main factors affecting the flow structure [4, 10-12]. In the rivers, roughness in the floodplain areas influences on the flow behavior; enhances the flow resistance and decreases the velocity [9, 13]. Experimental studies were carried out in the compound meandering channels with applications of urban fluvial and hydro-environment systems [14]. The results of relevant researches show that the geometry, displacement, and density of roughness have significant effect on the drag [15-17]. The effect of vegetation in the floodplain on the flow structure of the main channel was investigated using the flume experiments [9]. The results showed that the roughness significantly reduce the flow transfer capacity in the channel.

The flow structure in compound meandering channels under the effect of floodplain with one-sided vegetated was evaluated [18]. The results showed that the flow velocity in section with the maximum extension of vegetation in the floodplain is higher than the section with the minimum extension. Naghavi et al. [19] experimentally studied the flow structure in compound meandering channels under the effect of two-sided buildings density change. They discussed that at high relative flow depth (Dr=0.49), with the increase of two-sided buildings density of the floodplain by 23.7%, in the main channel, the dimensionless flow velocity increases by 61%, in comparison with the smooth condition of the floodplain. Furthermore, flow structures in the compound meandering channels under the different building arrangement was evaluated using experimental cases [20]. The results indicated that by arranging the construction barriers perpendicular to the flow of the floodplain, the velocity increases by 113% in comparison with the smooth case.

Equally important as experimental researches, numerical simulations can provide Additional findings (e.g., the flow direction and velocity magnitude) about the flow characteristics in meandering compound channels and the understanding of turbulent flow behavior is developed. High accuracy simulations for the flow characteristics such as the velocity distribution and depth ratio were reported using the several 2D and 3D numerical models [4, 8, 21]. Shukla and Shiono [21] evaluated the flow conditions in compound meandering channels by computational fluid dynamics (CFD) model. Their proposed numerical model provided high accuracy in predicting flow velocity, bed shear stress, water surface level and turbulent kinetic energy. The effects of trees and shrubs at the edge of a floodplain on flow hydrodynamics were investigated by Sanjou and Nezu [22]. They reported that the velocity reduces behind trees. Naghavi et al. [23] by investigating the boundary shear stress in meandering compound channels with one-sided

structural density, showed that the maximum bed shear stress moves towards the smooth floodplain in the middle sections.

In the past few decades, the frequency of occurrence of floods has increased due to climate change, population growth on the banks of rivers and industrialization. Thus, it is essential to understand the flooding problem by evaluating the physics behind that. However despite advancement of knowledge on hydrodynamics, the meandering compound channels supported by the huge amount of researches in laboratory and field conditions as well as by numerical models, the studies related to the complex flow structure by meandering compound channels with the various buildings located on the floodplains is still rare. In particular, the changes of the vortices and the characteristics of transverse flows have yet to be studied in-depth, which is the exact goal of this study. The present research work focuses to numerically evaluating the impact of building arrangement changes on the transverse flow velocity, vorticity and flow angle in the main channel using a Reynolds Renormalization Group (RNG) turbulent model. Naghavi et al. [24-29] showed that the RNG turbulent model has high accuracy in simulating the flow in meandering compound channels.

2. Materials and Methods

2.1. Experimental data

In this research, the laboratory data of Naghavi et al. [20] were used as a reference. The laboratory flume was 16 m in length, 2.07 m in width, and 0.40 m in height (see Figure 1). Naghavi et al. [20] used three different building arrangements according to Figure 1 and Table 1 to investigate the effect of structural arrangements on the flow patterns. In this study, the sinuosity of the main channel ($s = L/L_w$, being L the meandering channel length and L_w the meander wavelength) was 1.21, the valley slope (S_0) was 0.001, the overall width of the compound channel (B) was 2.07 m, the width of the meandering main channel (b) was 0.5 m and the channel depth (h) was 0.1 m. More details of the meandering compound channel geometry used in the experiments and the numerical model are shown in Figure 2, where B_m is the meander belt width, θ is the cross-over angle, θ_1 is the flow angle in the main channel and CS1 to CS7 is the measurement sections for the model meander. In Table 1, Q is the total discharge, H is the flow depth in the main channel, Dr [=(H-h)/H] is the relative flow depth, %St is the density of buildings, Fr ($=U_m/\sqrt{gR}$) is the Froude number, in which R is the hydraulic radius at apexes and Re ($=U_mR/\upsilon$) is the Reynolds number with the kinematic viscosity υ (=0.01 cm^2/s), U_m is the average velocity in the apex section.

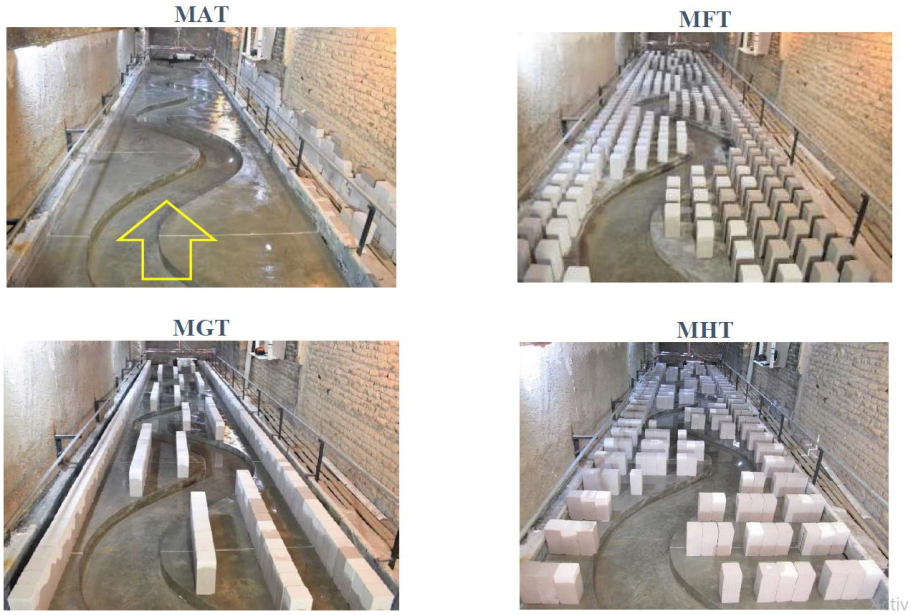

Figure 1. A view of the laboratory flume [20]

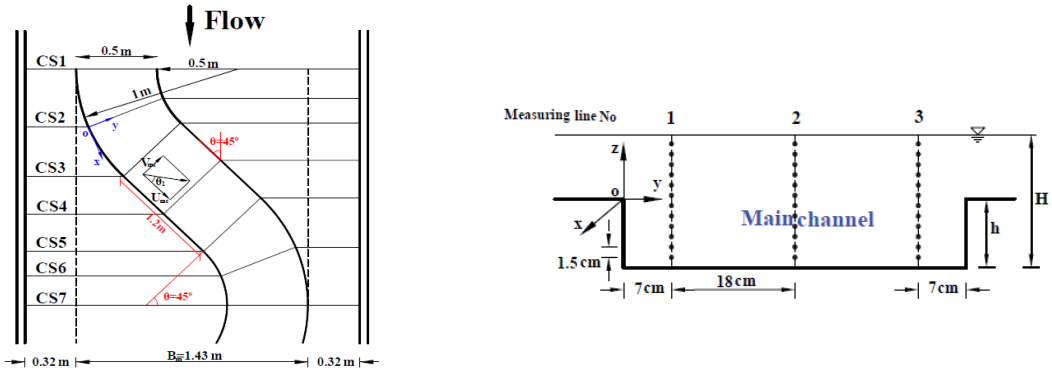

Figure 2. A plan view and measured sections

Table 1. Experimental parameters [20].

Case	Q(m^3/s)	H(cm)	Dr	%St	Fr	Re	n
MAT1	0.076	19.5	0.49	0	0.31	30691	0.022
MAT2	0.044	16.4	0.39	0	0.28	18182	0.024
MAT3	0.025	14.1	0.29	0	0.24	10502	0.026
MFT1	0.038	19.5	0.49	23.7	0.16	15528	0.044
MFT2	0.025	16.4	0.39	23.7	0.16	10425	0.041
MFT3	0.016	14.1	0.29	23.7	0.16	6930	0.039
MGT1	0.058	19.5	0.49	23.7	0.24	23415	0.029
MGT2	0.035	16.4	0.39	23.7	0.22	14721	0.029
MGT3	0.019	14.1	0.29	23.7	0.20	8418	0.032
MHT1	0.034	19.5	0.49	18.5	0.14	13943	0.049
MHT2	0.023	16.4	0.39	18.5	0.15	9591	0.045
MHT3	0.014	14.1	0.29	18.5	0.14	6122	0.044

2.2. Numerical models and governing equations

In this study, a CFD model was used to investigate numerically the transverse flow velocity, vorticity and the flow angle in meandering compound channels under the effect of changing the building arrangement. The channel dimensions and building arrangements in the numerical models are the same as the laboratory model by Naghavi et al. [20].

Herein, Flow3D software was used to model the meandering compound channel and investigate its flow behavior. Flow3D is capable to solve complex fluid dynamics problems, and user friendly as well as has a very powerful graphical interface that makes it easier to work with. This software uses Finite Volume Method to solve governing equations and using regular networking and volume of fluid methods to calculate free surface level in open channels. Flow3D software governs by Navier-Stokes momentum and continuity equations for the entire computing space. In Fig. 3, numerical models created for different building arrangements are shown. The governing continuity equation and the Reynolds-Averaged Navier–Stokes (RANS) equations are:

$$V_f \frac{\partial \rho}{\partial t} + \frac{\partial(\rho u A_x)}{\partial x} + \frac{\partial(\rho v A_y)}{\partial y} + \frac{\partial(\rho w A_z)}{\partial z} = R_{SOR} \quad (1)$$

$$\frac{\partial u}{\partial t} + \frac{1}{V_f}\left(uA_x \frac{\partial u}{\partial x} + vA_y \frac{\partial u}{\partial y} + wA_z \frac{\partial u}{\partial z}\right) = -\frac{1}{\rho}\frac{\partial P}{\partial x} + G_x + f_x \quad (2)$$

$$\frac{\partial v}{\partial t} + \frac{1}{V_f}\left(uA_x \frac{\partial v}{\partial x} + vA_y \frac{\partial v}{\partial y} + wA_z \frac{\partial v}{\partial z}\right) = -\frac{1}{\rho}\frac{\partial P}{\partial y} + G_y + f_y \quad (3)$$

$$\frac{\partial w}{\partial t} + \frac{1}{V_f}\left(uA_x \frac{\partial w}{\partial x} + vA_y \frac{\partial w}{\partial y} + wA_z \frac{\partial w}{\partial z}\right) = -\frac{1}{\rho}\frac{\partial P}{\partial w} + G_z + f_z \quad (4)$$

where, (u, v, w) are velocity components (m/s); (A_x, A_y, A_z) are flow area fractions; (G_x, G_y, G_z) are mass accelerations; and (f_x, f_y, f_z) are viscous accelerations in (x, y, z) directions, ρ is the fluid density, R_{SOR} is the spring term, V_f is the fraction of the volume associated with the flow, and P is the pressure (N/m^2).

In this study, the flow turbulence was represented by solving the RANS equations using the Reynolds Renormalization Group (RNG) turbulent model. A review of numerical studies shows that the RNG model can accurately predict the Reynolds shear stress and can generate secondary properly [30, 31]. According to Yakhot *et al.* [32], the equations for the RNG turbulent model are as follows:

$$\frac{\partial k}{\partial t} + \bar{u}_i \frac{\partial k}{\partial x_i} = \nu_t \, S^2 - \epsilon + \frac{\partial}{\partial x_i}\left(\alpha \, \nu_t \frac{\partial k}{\partial x_i}\right) \quad (5)$$

$$\frac{\partial \epsilon}{\partial t} + \bar{u}_i \frac{\partial \epsilon}{\partial x_i} = C_{\epsilon 1} \frac{\epsilon}{k} \nu_t \, S^2 - C_{\epsilon 2} \frac{\epsilon^2}{k} - R + \frac{\partial}{\partial x_i}\left(\alpha \, \nu_t \frac{\partial \epsilon}{\partial x_i}\right) \quad (6)$$

where, k is the turbulent kinetic energy, ϵ the dissipation rate, ν_t the turbulent eddy viscosity, S^2 the magnitude of the strain rate, $R = \frac{C_\mu \eta^3 (1-\eta/\eta_0)}{1+\beta \eta^3}\frac{\epsilon^2}{k}$, $\eta = \frac{Sk}{\epsilon}$ factors of C_μ $C_{\epsilon 1}$, $C_{\epsilon 2}$, η_0, α, and β are constants, and their values are listed in Table 2. For tracking and locating the free surface flow, the volume of fluid (VOF) method was used. This technique belongs to the class of Eulerian method based on the idea of a fraction

function, $F(x, y, z, t)$, indicating the ratio of the volume occupied by the fluid to the total volume of a grid. Three considered cases were: (*i*) the cell is empty, F=0; (*ii*) the cell is full, F=1; and (*iii*) in the cell is a fluid interface, 0<F<1.

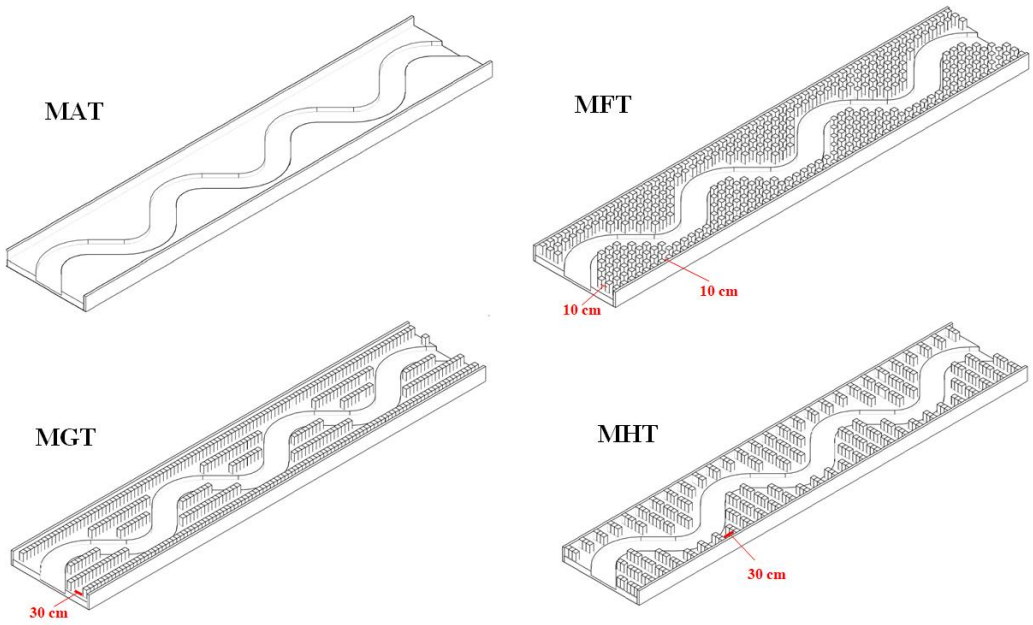

Figure 3. Numerical models created for different building arrangements

Table 2. Coefficients for the RNG turbulent model [32].

C_μ	$C_{\epsilon 1}$	$C_{\epsilon 2}$	η_0	α	β
0.085	1.42	1.68	4.38	1.39	0.012

2.3. Boundary conditions and model gridding

The boundary conditions of numerical model are the same as physical model used in Naghavi *et al.* [20]. Boundary conditions of volume flow rate and specified pressure were defined in the entrance and exit of the meandering compound channel, respectively. Wall boundary conditions were used for the bed and sidewalls of the channel. For the free surface, a symmetry boundary condition was applied [8]. Fig. 4 shows the boundary conditions of the flow domain.

The FLOW-3D model employs cubic cells (regular grids). To obtain accurate results, the optimal grid spacing was determined by checking mesh quality based on the adjacent cell size ratio and the aspect ratio. The optimal ratios are close to 1. The maximum of adjacent cell size ratio and the aspect ratio do not exceed 1.25 and 3, respectively. Consequently, the meshes were re-adjusted so that the limits of the ratios were satisfied. Furthermore, the grid was refined to reduce errors of the numerical model (Table 3). It was found that the model with very fine grids has a lower mean absolute percentage error (MAPE, %) than the other models. In addition, results obtained by fine grids are very similar to those by very fine grids. Grid-independent results suggested that fine grids ensure a reasonable accuracy, so this grid was used for all simulations. The grid resolution determining method used here are similar to those in the literature [8, 31, 33, 34, 35]. The MAPE (%) and the root mean square error (RMSE) for each quantity are calculated by equations (7) and (8) below:

$$MAPE = 100 \times \frac{1}{n} \sum_{i=1}^{n} \left| \frac{E_i - N_i}{E_i} \right| \quad (7)$$

$$RMSE = \sqrt{\frac{1}{n} \sum_{i=1}^{n} (E_i - N_i)^2} \quad (8)$$

where, E_i is the value of experimental data, N_i is the value of numerical data, and n is a number of data.

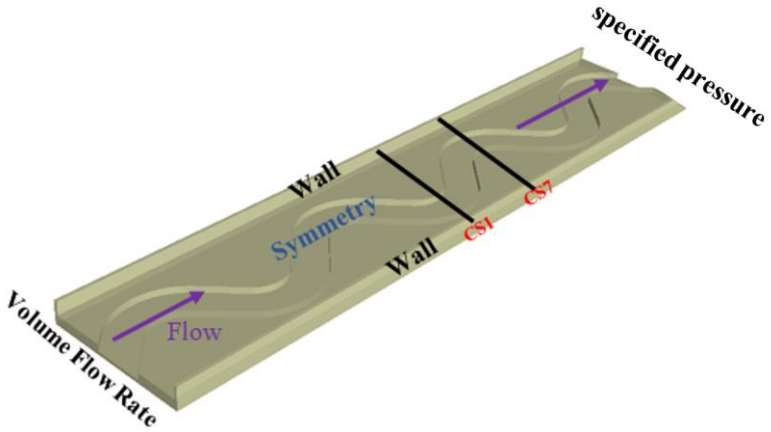

Figure 4. Boundary conditions for the flow domain.

Table 3. The accuracy of different model grids based on the mean absolute percentage error (MAPE, %) of depth-averaged velocities calculated in sections CS1 and CS4 for cases MAT1, MFT1, MGT1 and MHT1

Type of gridding	Grid spacing (cm)	MAPE (%)							
		MAT1		MFT1		MGT1		MHT1	
		CS1	CS4	CS1	CS4	CS1	CS4	CS1	CS4
Coarse	3	8.82%	9.17%	9.86%	10.24%	10.11%	10.66%	10.89%	11.26%
Medium	1.5	5.93%	6.21%	6.84%	7.16%	7.09%	7.46%	7.73%	7.95%
Fine	1	3.55%	3.96%	4.45%	4.96%	4.54%	4.99%	5.04%	5.22%
Very Fine	0.75	3.53%	3.94%	4.42%	4.93%	4.51%	4.95%	5.01%	5.18%

2.4. Model validation

In present research work, to validate the results of numerical model, the values of Q_{mc}/Q (the ratio of main channel discharge to the total discharge), depth-averaged velocity and longitudinal flow velocity in different sections of the main channel were compared with the laboratory model results of Naghavi et al. [20]. Fig. 5 shows the comparison of experimental and numerical results for Q_{mc}/Q at sections CS1-CS7 for cases with various structural arrangements in Dr= 0.49. As can be seen in the figure, the trend of the graph for each of the numerical results is similar as the experimental results. The RMSE error values for cases MAT1, MFT1, MGT1 and MHT1 are 0.010, 0.017, 0.013 and 0.024, respectively, and the MAPE error values are 2.86%, 3.01%, 3.05% and 3.24% respectively, which shows an acceptable agreement between the numerical and experimental results. Fig. 6 shows the comparison of experimental and numerical results for

depth-averaged velocities in section CS1 for cases with different building arrangements. The RMSE and MAPE error values have been measured in each of the graphs. The results show that the calculated depth-averaged velocities are in reasonable agreement with the experimental data measured for all cases.

Fig. 7 shows the experimental and numerical results for longitudinal flow velocity (U) in cases MAT1 and MFT1 and sections CS1 and CS4. According to the figure, the simulated velocity profile reproduces corresponding results to the experimental data. The RMSE and MAPE error values also reconfirm this agreement between the numerical and experimental results. De Marchis and Napoli [36] and Xu *et al*. [33] numerically computed the complex properties of three-dimensional flows in meandering compound channels, and they showed similar discrepancy of their simulations to actual measurements in most compared cases.

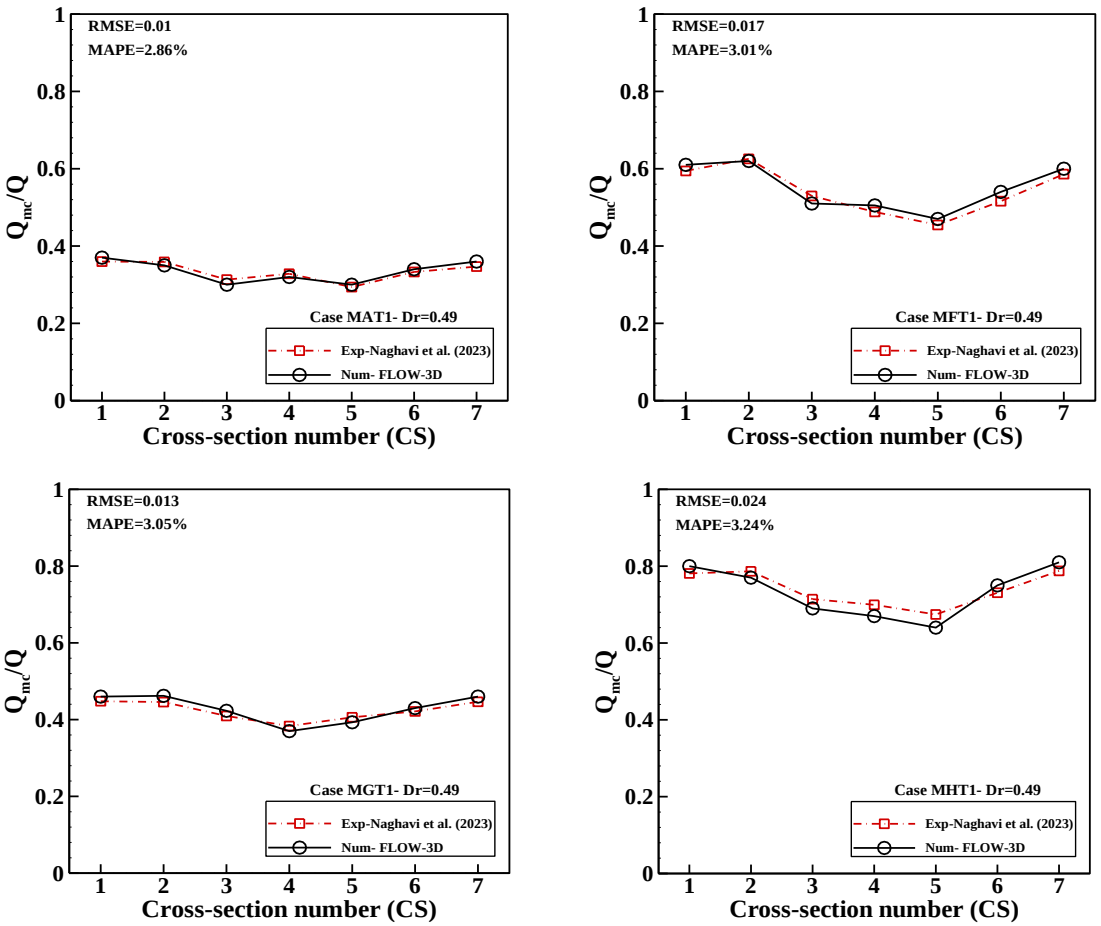

Figure 5. Experimental and numerical results of Q_{mc}/Q in relative depth of 0.49

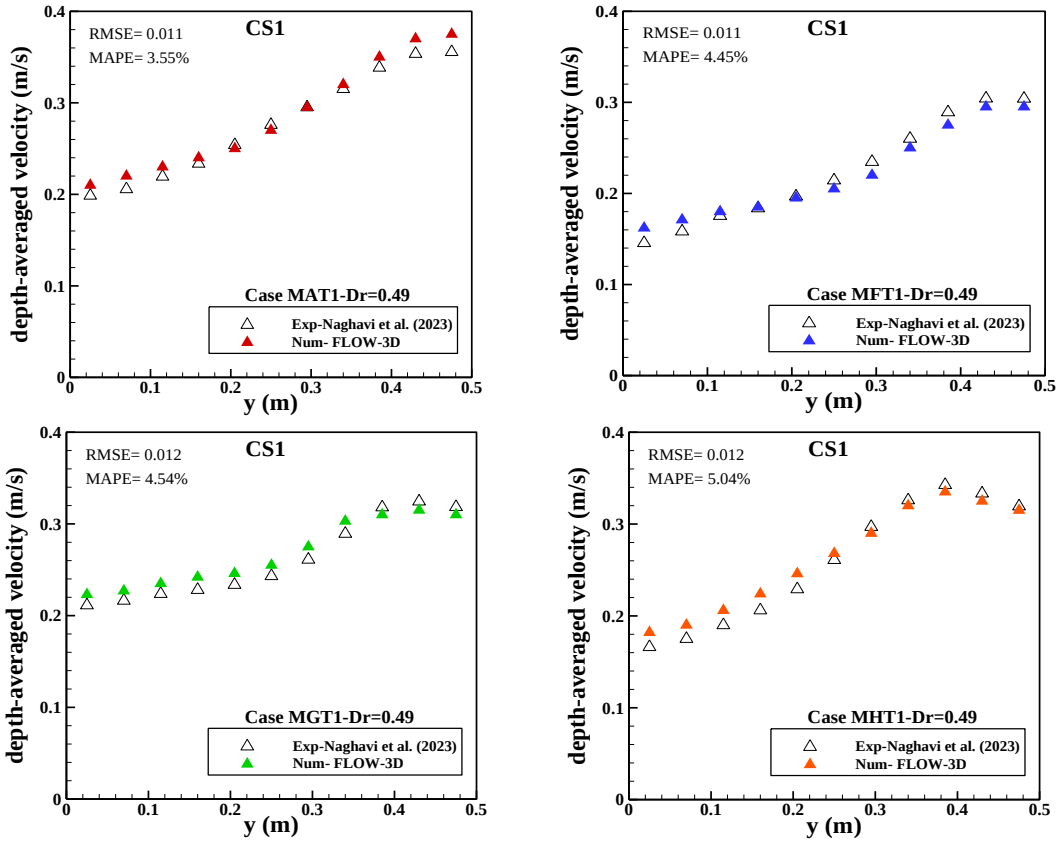

Figure 6. A comparison of experimental and numerical results for depth-averaged velocities in section CS1 and relative depth of 0.49

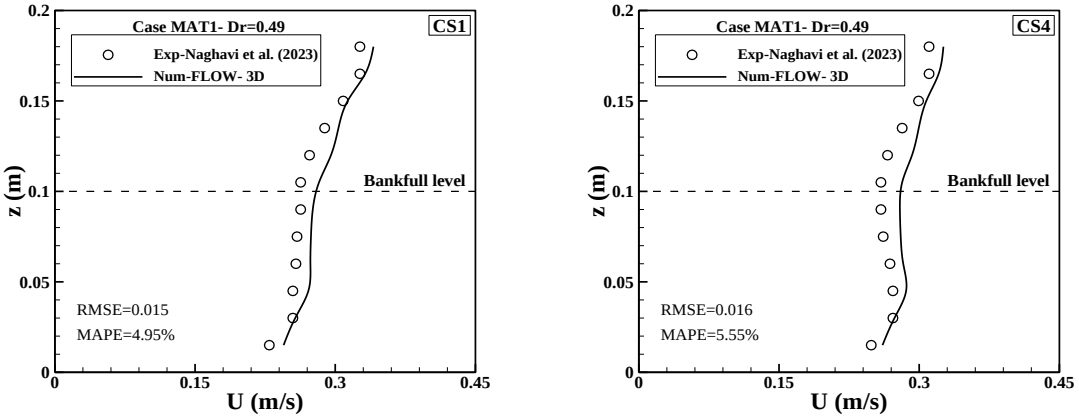

Figure 7. A comparison of experimental and numerical results for longitudinal flow velocity (U) in cases MAT1 and MFT1 and sections CS1 and CS4

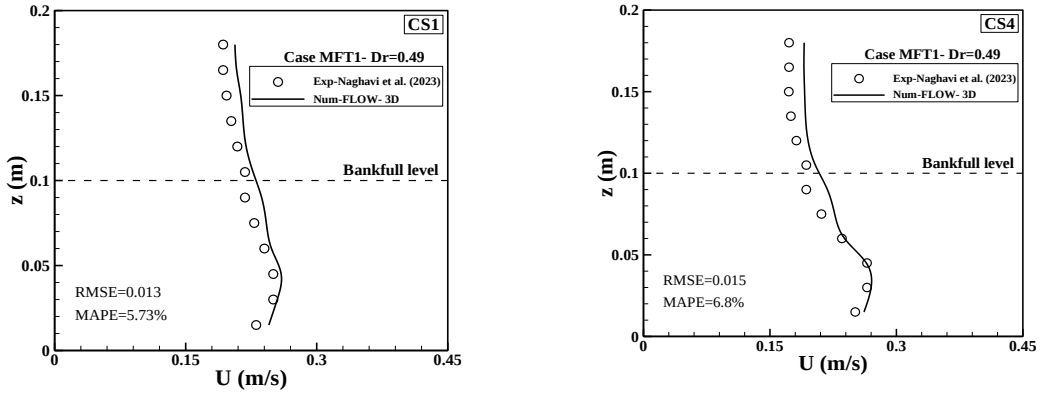

Figure 7. Continued

3. Results and Discussion

3.1. Transverse flow velocity

In Fig. 8, the distributions of the transverse flow velocity in the direction of flow depth (z) are shown with distances of 0.07, 0.25 and 0.43 meters at Dr= 0.49 for different buildings arrangement (see Figs. 2 and 10). In CS1 and CS7, considering that the deviation angle of main channel compared to the floodplain is zero (θ=0°), where the floodplain flow has negligible impact on the transverse velocity, and the main strength of the transverse flow in those sections is dependent on the centrifugal force. The transverse flow due to the centrifugal force is directed towards the outer arc (concave wall) at the bottom of the main channel and towards the inner arc (convex wall) at the water surface. At these sections, changing the arrangement of buildings in the floodplain leads to a change in the velocity values, and as a result, the centrifugal force changes in the main channel. In the concave arc of CS1 and CS7 (at the distance of 0.07 meter from the left wall of section CS1; and at a distance of 0.43 meters from the left wall of section CS7), variation of the buildings arrangement has a negligible effect on the transverse velocity. Near the convex arc of sections CS1 and CS7 (at a distance of 0.43 meters from the left wall of section CS1 and at a distance of 0.07 meters from the left wall of section CS7), changing the arrangement of buildings has a significant effect on the transverse velocity, because at those location, the flow velocity has the highest value and the transverse velocity will have the greatest changes due to the centrifugal force. In comparison, these changes in the concave arch are insignificant. In the apex sections (CS1,7), the transverse flow direction in the top and bottom of the bankfull level for MGT1 and MAT1 is different in the entire width of the section, which causes the creation of a secondary flow cell in these sections; however in MFT1 and MHT1, the transverse flow direction at the top and bottom of the bankfull level near the convex arc of sections CS1 and CS7 is not different, which indicates that the secondary flow cell in these channels do not cover the entire width of the section, and the secondary flow cell is formed only near the concave arc.

By moving away from the apex sections (CS1 and CS7), the flow of the main channel and floodplain will no longer be parallel to each other. In these sections, the transverse flows will be affected by the flow of the floodplain, besides the centrifugal force. According to Fig. 8, with the increase of the deviation angle of the main channel with respect to the floodplain (from zero degrees in apex sections to 22.5 degrees in sections CS2 and CS6), the value of the transverse velocity increases for sections CS2 and CS6.

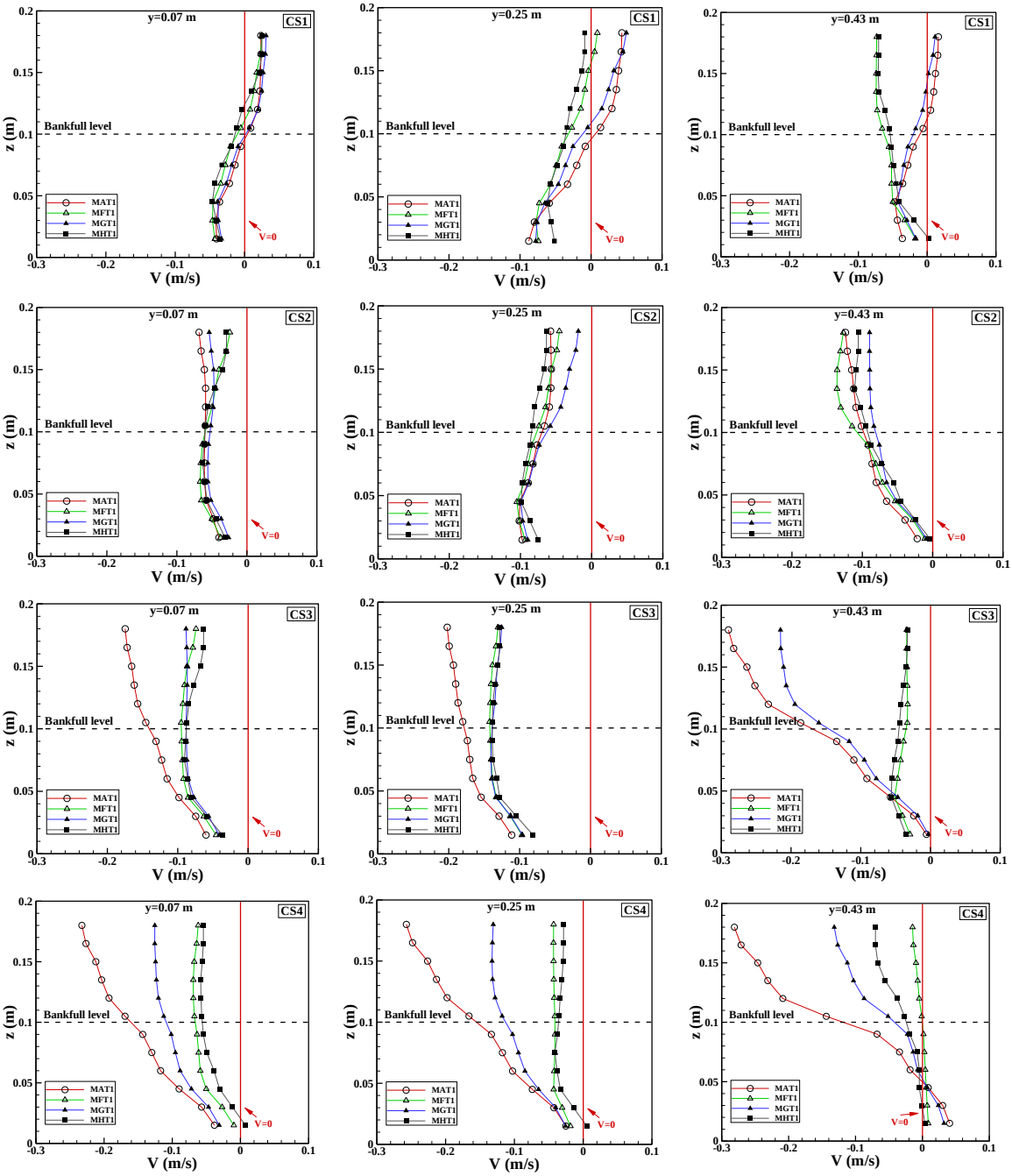

Figure 8. The distributions of transverse velocity in the direction of flow depth in three axes with distances of 0.07, 0.25 and 0.43 meters in Dr= 0.49

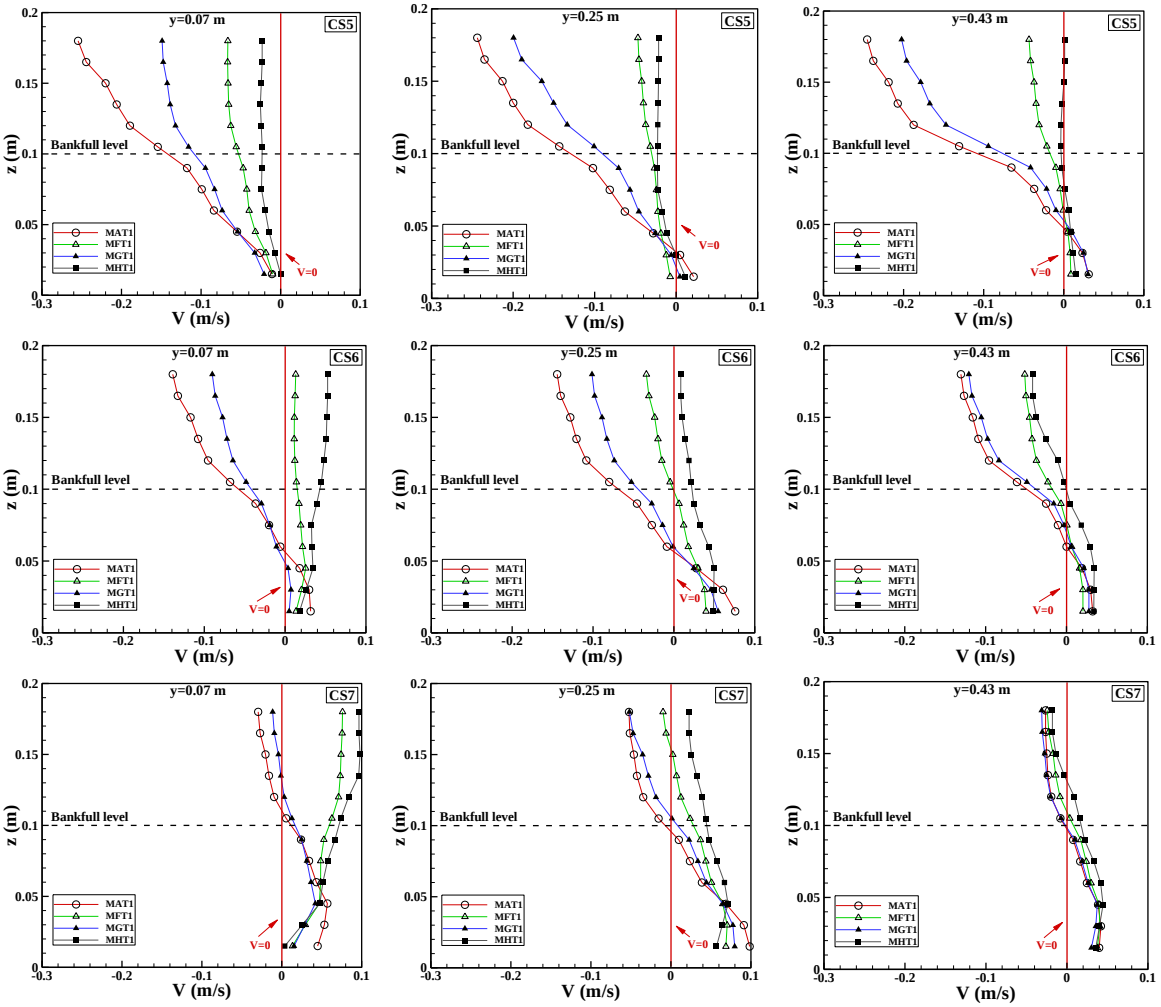

Figure 8. Continued

According to Fig. 9, in section CS2, considering that the direction of the flow caused by the centrifugal force (v_1) and by the floodplain flow passing over the main channel (v_2), they are opposite to each other. The transverse flow velocity above the bankfull level is lower than the CS6 section, therefore, changing the arrangement of the building has a negligible effect on the alteration of transverse flow velocity characteristic. As can be seen in Figs. 8 and 9, in section CS2, considering that the direction of transverse flows at the top and bottom of the bankfull level is the same, no secondary flow cell is formed in this section. However in section CS6, considering that the direction of transverse flows is different at the top and bottom of the bankfull level, a secondary flow cell is created in this section. In section CS6, the direction of transverse flows above and below the bankfull level is different for the MAT1, MFT1 and MGT1 channels, and the cell of secondary flows covers the entire width of the section, but in case MHT1, the direction of transverse flows at the top and bottom of the bankfull level is different at y=0.43 m, and the secondary flow cell is formed in the right half of the section only. Referring to Fig. 8, in case of mid sections (CS3, CS4 and CS5), since the deviation angle of the main channel in compared with the floodplain has the highest value (θ=45°), the lateral flow of the floodplain ($U_{fp}(y)=U_{fp}Sin\theta$) has the greatest effect on the transverse velocity, especially

above the bankfull level. Therefore, in those sections, the building arrangements are very important, e.g. in cases MFT1 and MHT1, with a decrease of the floodplain flow velocity (U_{fp}), the transverse velocity (V) decreases significantly. In the CS4 section, the maximum transverse velocity in MFT1, MGT1 and MHT1 cases is reduced by 84%, 49% and 80% on average compared to the MAT1 case.

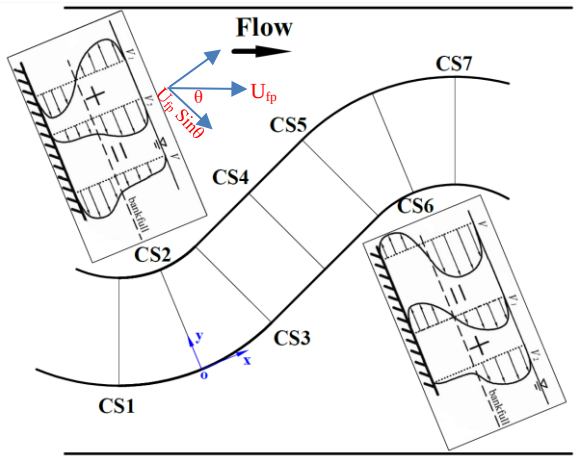

Figure 9. The trend of transverse flow velocity distribution in the center of the main channel for sections CS2 and CS6

3.2. Flow angle in the main channel

In Fig. 10, the flow angle relative to the meandering channel wall (θ_1) is calculated as θ_1=arctan(v/u). In this figure, the angles θ_x and θ_{geo} are the cross-section angle and the bending angle of meandering channel, respectively. In Fig. 11, the changes of angle θ_1 in the direction of depth (z) in three axes with distances of 0.07, 0.25 and 0.43 meters at Dr= 0.49 are shown according to the change of building arrangements. Also can be seen in this figure, the effect of floodplain flow on the transverse velocity in the main channel (v) is insignificant in sections CS1, 7 (with θx=0), and changing the arrangement of the building has very little effect on the vertical distribution of θ_1 near the concave arc. But considering that the maximum velocity occurs in the convex arc and with the change of velocity as well as the change of the centrifugal force, the changes of angle θ_1 are more noticeable, so that the flow angle θ_1 above the bankfull level of MFT1 and MHT1 is greater than MAT1 and MGT1.

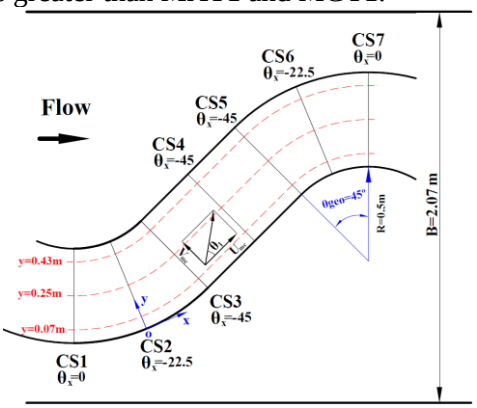

Figure 10. The geometrical plan of meandering compound channel and flow angle

In the CS2 section, changing the arrangement of the building has no noticeable effect on the flow angle; and the smallest flow angle in case MGT1 occurs near the right wall. In the same section, the directions of transverse flows caused by the centrifugal force and the floodplain flow above the bankfull level are opposite to each other. As a result, the transverse velocity and the angle θ_1 above the bankfull level are lower than in section CS6. Also, the change in the building arrangement has less effect on the change of angle θ_1 above the bankfull level. In sections CS2 and 6, the flow velocity near the convex arc is greater than the concave arc, leading to the greater effect by variation of the building arrangement on the angle θ_1. In section CS6, since the flow enters the floodplain from near the left wall (y=0.07m), the building arrangement and obstacles created in the floodplain has a great effect on the angle θ_1 when the flow exits this location.

In sections CS3, CS4 and CS5, due to the deviation angle of meandering channel is great compared to the floodplain flow, the effect of the transverse flow of the floodplain in these sections is significant. At these sections, the change of building arrangement has a considerable effect on the angle, so that near the entrance of the floodplain flow (y=0.43m), the flow angle θ_1 is the highest above the bankfull level. By moving towards the outlet of the flow from the main channel to the floodplain (y=0.07m), its value decreases. Near the left wall (y=0.07m) where the flow exits from the main channel to the floodplain, the MHT1 channel creates more resistance during flow exits, causing the value of the flow angle θ_1 to reduce in this location. Near the left wall and the center of the meandering channel, the variation of the angle θ_1 in the depth direction for case MHT1 is insignificant; but in case MGT1, the variation of the angle θ_1 in the direction of the flow depth is high due to the intensity of the floodplain flow passing over the meandering channel, and the maximum value of θ_1 occurs above the bankfull level. These angle changes along the flow depth have been observed correspondingly in the studies conducted by Shan et al. [37] and Liu et al. [38].

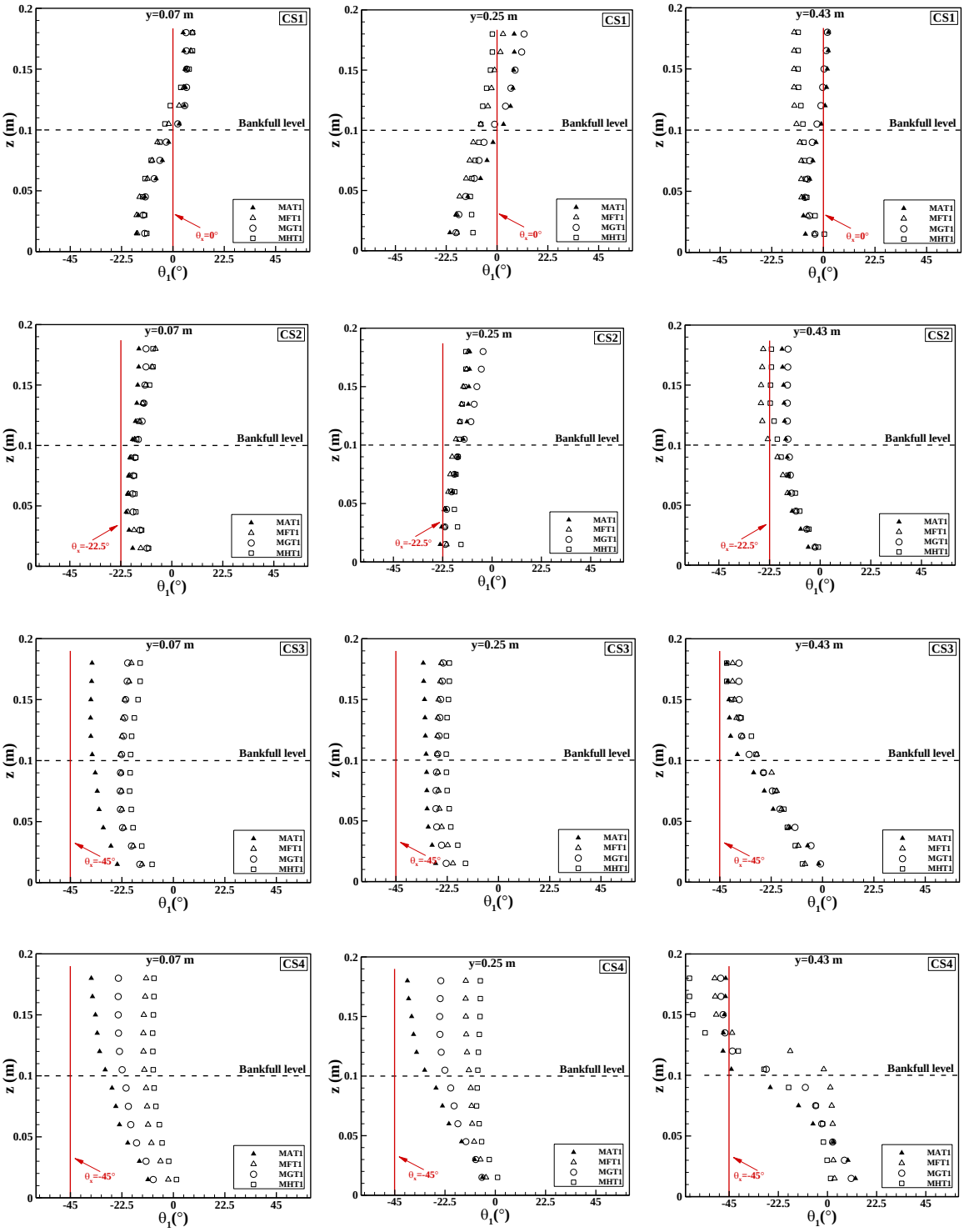

Figure 11. Variations of the angle θ_1 in the direction of depth (z) at three axes for different building arrangements

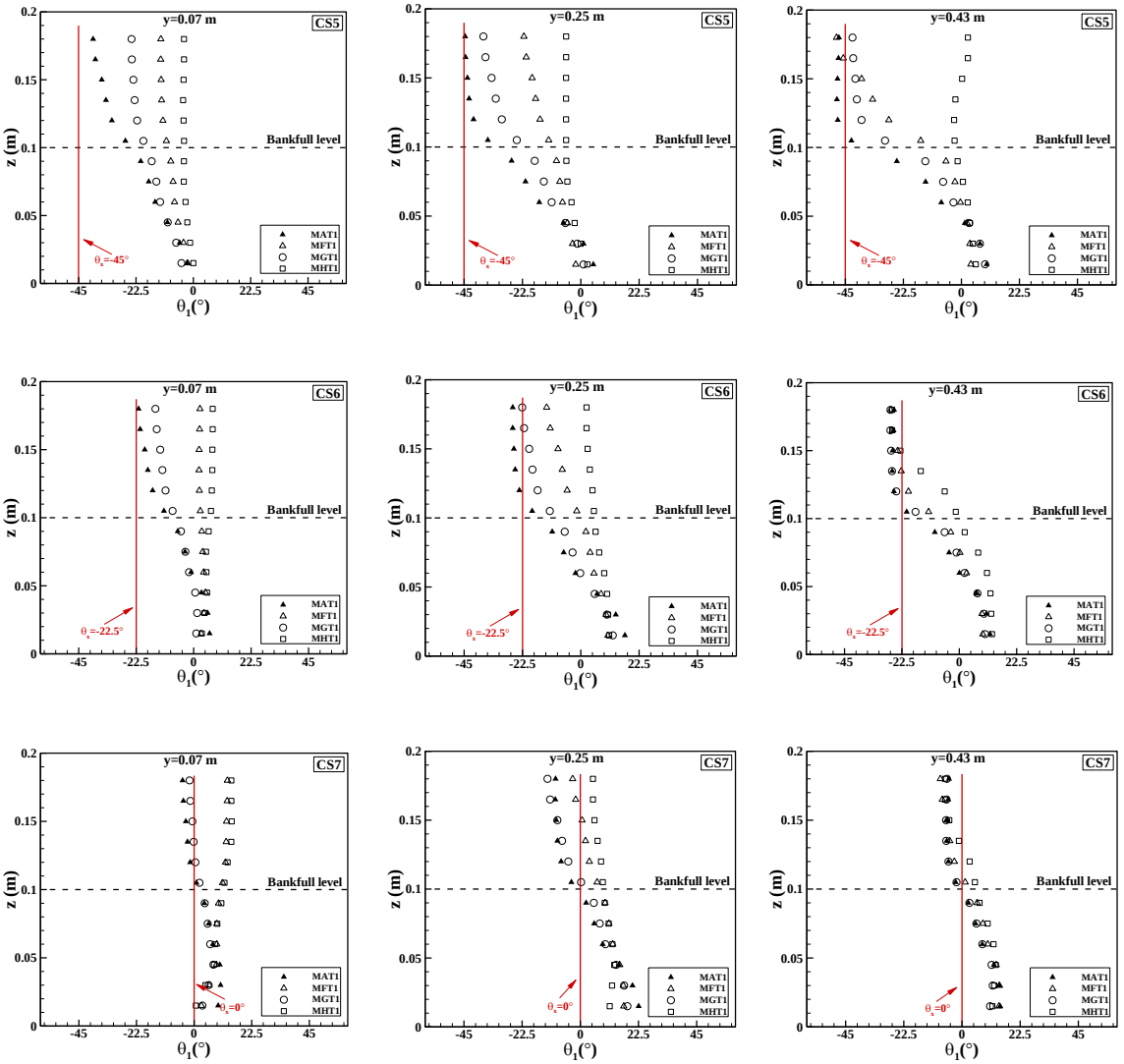

Figure 11. Continued

3.3. Vorticity

Transverse flows in meandering compound channels create vortices where the net rate of counter-clockwise rotation of an element with dimensions $\Delta y \times \Delta z$ around the x-axis is defined as $\bar{\omega}_x = 1/2(\partial w/\partial y - \partial v/\partial z)$, where ω_x is the amount of rotation around the x-axis and *v* and *w* are the velocity components in the direction of the *y* and *z* axes. In Fig. 12, the vorticity created around the x-axis at various cross sections under the building arrangement variation at Dr=0.49 is displayed. In the figure, dashed lines indicate negative values of vortices (clockwise) and solid lines indicate positive values of vortices (counter-clockwise). Variation of the building arrangement in sections CS1 and CS7 has the greatest effect near the inner arc (convex arc) on the rotation strength of the vortices. In sections CS1 and CS7, the maximum velocity appears near the convex arc, so by changing the arrangement of the building, velocity and centrifugal force, the rotation strength of the vortices experiences more drastic changes. In the middle sections (CS3, CS4 and CS5), by increasing the deviation angle of the meandering channel compared to the floodplain, the effect of the transverse floodplain flow is dominant. The change of building arrangement due to the obstacles that create in front of the floodplain flow has a great effect on the rotation strength of the vortices, and in case MGT1, the strength of vortices rotation increases significantly compared to case MHT1. The arrangement of structural barriers in case MGT1 is such that it can easily transfers the flow of the floodplain, but in case MHT1, the intensity of the transverse flow is significantly reduced due to the arrangement of the building perpendicular to the flow of the floodplain. These changes are more noticeable at the entrance of the floodplain flow to the main channel near the right wall.

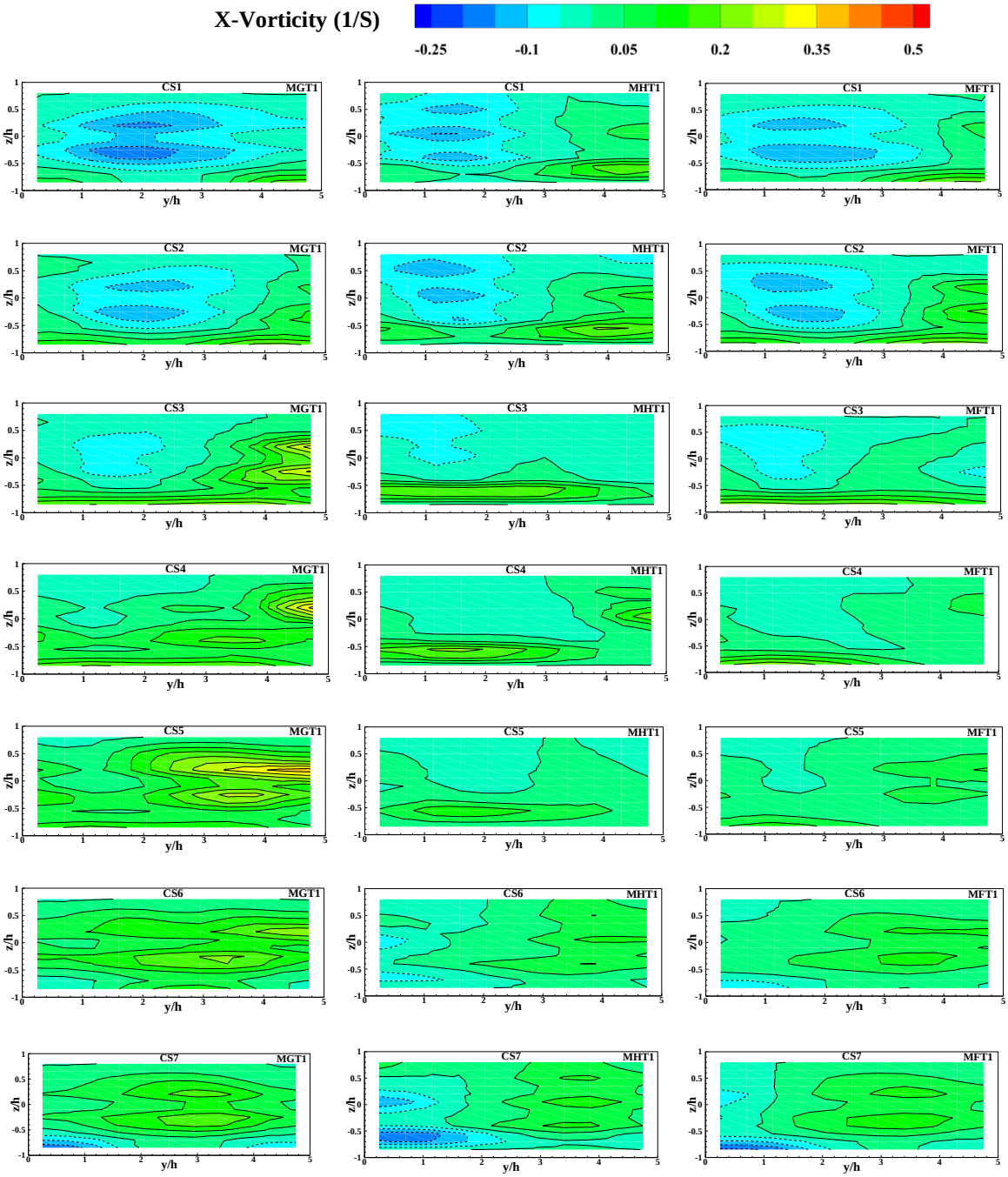

Figure 12. The variations of vorticity for different cases

4. Conclusions

In present research work, the behavior of transverse flow velocity, flow angle and vortices in meandering compound channels under the effect of changing building arrangement was investigated. For this purpose, three different building arrangements have been used, and the results have also been compared with smooth floodplains. Measurements were acquired in seven sections along the meandering main channel for different relative depths. Summary of the findings are:

1- In apex sections (i.e., CS1 and CS7), the flow of floodplain had a negligible effect on the transverse velocity of those sections dependent on the centrifugal force. In the concave arc of sections CS1 and CS7, variation of the buildings arrangement had a negligible effect on the transverse velocity. Near the convex arc in apex sections, the buildings arrangement had an extreme effect on the transverse flow velocity.
2- In section CS2, the transverse velocity above the bankfull level is lower than the CS6 section; therefore, building arrangement variation had less effect on the change of transverse velocity.
3- In the middle sections, variation of the buildings arrangement had a considerable effect on the transverse velocity, where in the CS4 section, the maximum averaged transverse velocity in MFT1, MGT1 and MHT1 cases decreases by 84%, 49% and 80%, respectively, compared to the smooth floodplain.
4- In sections (CS3, CS4 and CS5), building arrangement variation had a significant effect on the flow angle, where the flow of the floodplain enters to the meandering channel (y=0.43m), the flow angle θ_1 is the highest above the bankfull level, and by moving towards the outlet of the flow from the main channel to the floodplain (y=0.07m), its value decreases.
5- In the middle sections (CS3, CS4 and CS5), variation of the building arrangements had a considerable effect on the rotation strength of the vortices, thus in case MGT1, the strength of vortices rotation increases significantly compared to case MHT1.
6- According to the results of this research and due to the clarity of the building arrangements in each region through satellite photos, it is possible to make the necessary predictions before the flood occurs. For example, before the flood, sections of the river that need to be dredged for the flood flow to pass through the city have been identified so that more flood flow leaves the city. Also, according to the results of this research, it is possible to predict the water level and flood extent in each region according to the arrangement of the buildings, and determine how the flood flow will pass through the river and floodplain, and determined when the flood flow will leave the city under these conditions.

Statements and Declarations

Ethical Approval, Consent to Participate, and Consent to Publish: *The authors confirm that this manuscript describes an original work and has not yet been published or presented elsewhere in part or in entirety, and is not under consideration by another journal. Authors of the paper have also approved the manuscript and agree with submission of the paper to the* **"Journal of Hydraulic Structures".**

Funding*: The authors declare that no funds, grants, or other support were received during the preparation of this manuscript.*

Competing Interests: *The authors have no relevant financial or non-financial interests to disclose.*

Author Contributions: *All authors contributed to the study conception and design. Material preparation, data collection and analysis were performed by Mohammad Naghavi, Mirali*

Mohammadi, and Ghorban Mahtabi. The first draft of the manuscript was written by Mohammad Naghavi and all authors commented on previous versions of the manuscript. All authors read and approved the final manuscript.

Availability of data and materials: *Some or all data used during the study are available from the corresponding author upon reasonable request.*

References

1. Knight DW, Demetriou JD, (1983). Floodplain and main channel flow interaction. Journal of Hydraulic Engineering, 109(8), 1073–1092.
2. Liu C, Wright N, Liu X, Yang K, (2014). An analytical model for lateral depth-averaged velocity distributions along a meander in curved compound channels. Advances in Water Resources, 74, 26-43.
3. Shiono K, Muto Y, (1998). Complex flow mechanisms in compound meandering channels with overbank flow. Journal of Fluid Mechanics, 376, 221–261.
4. Ismail Z, (2007). A study of overbank flows in non-vegetated and vegetated floodplains in compound meandering channels. Dissertation for the Doctoral Degree. Loughborough: University of Loughborough.
5. Zhang HT, Dai WH, da Silva AMF, Tang H, (2022). Numerical study on resistance to flow in meandering channels. Journal of Hydraulic Engineering, 148, 1–14.
6. Pu JH, (2019). Turbulent rectangular compound open channel flow study using multi-zonal approach. Environmental Fluid Mechanics, 19(3), 785-800.
7. Pu JH, (2022). Editorial: Environmental Hydraulics, Turbulence and Sediment Transport. Fluids (MDPI), 7(48), 1-2.
8. Moncho-Esteve I, Palau-Salvador G, García-Villalba M, Muto Y, Shiono K, (2018). A numerical study of the complex flow structure in a compound meandering channel. Advances in Water Resources, 116, 95–116.
9. Liu C, Shan Y, Liu X, Yang K, Liao H, (2016). The effect of floodplain grass on the flow characteristics of meandering compound channels. Journal of Hydrology, 542, 1-17.
10. Tsujimoto T, (1992). Spectral analysis of velocity and water surface fluctuations appearing in an open channel with vegetated and non-vegetated regions in a cross-section. In: Proceedings of the sixth IAHR International Symposium on Stochastic Hydraulics, IAHR, Taipei.
11. Zhang HT, Dai WH, da Silva AMF, Tang HW, (2021). Numerical model for convective flow in meandering channels with various sinuosities. Journal of Hydraulic Engineering, 147, 04021042.
12. Mahato RK, Dey S, Ali SZ, (2022). Planform evolution of a sinuous channel triggered by curvature and autogenic width oscillations due to generic grain transport. Physics of Fluids, 34, 044110.
13. Wang M, Avital EJ, Bai X, Ji C, Xu D, Williams JJR, Munjiza A, (2020). Fluid–structure interaction of flexible submerged vegetation stems and kinetic turbine blades. Computational Particle Mechanics, 7, 839–848.

14. Pu JH, Pandey M, Li J, Satyanaga A, Kundu S, Hanmaiahgari PR, (2022). Editorial: Urban Fluvial and Hydro-Environment System. Frontiers in Environmental Science, 10(1075282)1-3.
15. Tang H, Tian Z, Yan J, Yuan S, (2014). Determining drag coefficients and their application in modelling of turbulent flow with submerged vegetation. Advances in Water Resources, 69, 134–145.
16. Pu JH, Hussain A, Guo Y, Vardakastanis N, Hanmaiahgari PR, Lam D, (2019). Submerged Flexible Vegetation Impact toward Open Channel Flow Velocity Distribution: An Analytical Modelling Study on Drag and Friction. Water Science Engineering, 12(2), 121-128.
17. Kundu S, Chattopadhyay T, Pu JH, (2022). Analytical models of mean secondary velocities and stream functions under different bed-roughness configurations in wide open-channel turbulent flows. Environmental Fluid Mechanics, 22(1), 159-188.
18. Pan Y, Li Zh, Yang K, Jia D, (2019). Velocity distribution characteristics in meandering compound channels with one-sided vegetated floodplains. Journal of Hydrology, 578, 1-11.
19. Naghavi M, Mohammadi M, Mahtabi G, (2022). An experimental evaluation of the blocks in floodplain on hydraulic characteristics of flow in a meandering compound channel. Journal of Hydrology, 612, 1-20.
20. Naghavi M, Mohammadi M, Mahtabi G, (2023). The effect of building arrangement on the flow characteristics in meandering compound channels. Journal of Environmental Management, 331(1), 117288.
21. Shukla DR, Shiono K, (2008). CFD modelling of meandering channel during floods. Proceedings of the Institution of Civil Engineers-Water Management, 161, 1–12.
22. Sanjou M, Nezu I, (2010). Large eddy simulation of compound open-channel flows with emergent vegetation near the floodplain edge. Journal of Hydrodynamics, 22(5), 582-586.
23. Naghavi M, Mohammadi M, Mahtabi G, Abraham J. (2023). Experimental assessment of velocity and bed shear stress in the main channel of a meandering compound channel with one-sided blocks in floodplain. Journal of Hydrology, 617, 129073.
24. Naghavi M, Mohammadi M. A, Mahtabi G. (2019). Flow Velocity in Meandering Compound Channel under the Influence of Sinusoidal Change. Modares Civil Engineering journal, 19(5), 208-219.
25. Naghavi M, Mohammadi M, Mahtabi G. (2020). Turbulence Intensity and Boundary Shear Stress in Meandering Compound Channel under the Influence of Sinusoidal Changes. Journal of Modeling in Engineering, 18(60), 53-69.
26. Naghavi M, Mohammadi M, Mahtabi G. (2021). Numerical simulation of flow velocity distribution and shear stress in meandering compound channels. Iranian Water Researches Journal, 15(1), 23-34.
27. Naghavi M, Mohammadi M, Mahtabi G. (2021). Transverse Flow Characteristics in the Meandering Compound Channels. Amirkabir Journal of Civil Engineering, 53(8), 3499-3516.

28. Naghavi M, Mohammadi M, Mahtabi G. (2021). On the effect of relative flood depth on flow hydraulics in meandering compound channels. Irrigation and Water Engineering, 11(3), 55-78.
29. Naghavi M, Mohammadi M, Mahtabi G. (2023). The effect of structures density in the banks of meandering rivers on the flow characteristics during floods. Journal of Water and Irrigation Management.
30. Pu JH, Shao S, Huang Y, (2014). Numerical and experimental turbulence studies on shallow open channel flows. Journal of Hydro-environmental Research, 8(1), 9-19.
31. Pu JH, (2015). Turbulence Modelling of Shallow Water Flows using Kolmogorov Approach. Computational Fluids, 115, 66-74.
32. Yakhot V, Thangam S, Gatski TB, Orszag SA, Speziale CG, (1992). Development of turbulence models for shear flows by a double expansion technique. Physics Fluids, 4(7), 1-24.
33. Xu D, Bai Y, Munjiza A, Avital E, Williams J, (2013). Investigation on the Characteristics of Turbulent Flow in a Meandering Open Channel Bend Using Large Eddy Simulation. In: Proceedings of 2013 IAHR World Congress, IAHR, China.
34. Van CP, Deleersnijder E, Bousmar D, Soares-Frazão S, (2014). Simulation of flow in compound open-channel using a discontinuous Galerkin finite-element method with Smagorinsky turbulence closure. Journal of Hydro-environmental Research, 8(40), 396-409.
35. Brevis W, García-Villalba M, Niño Y, (2014). Experimental and large eddy simulation study of the flow developed by a sequence of lateral obstacles. Environmental Fluid Mechanics, 14, 873–893.
36. De Marchis M, Napoli E, (2008). The effect of geometrical parameters on the discharge capacity of meandering compound channels. Advances in Water Resources, 31, 1662–1673.
37. Shan Y, Huang S, Liu C, Guo Y, Yang K, (2018). Prediction of the depth-averaged two-dimensional flow direction along a meander in compound channels. Journal of Hydrology, 565, 318–330.
38. Liu X, Zhou Q, Huang S, Guo Y, Liu C, (2018). Estimation of flow direction in meandering compound channels. Journal of Hydrology, 556, 143-153.